https://doi.org/10.5194/egusphere-2025-3449
Preprint. Discussion started: 8 August 2025

Upscaling of soil methane fluxes from topographic attributes derived from a digital elevation model in a cold temperate mountain forest

Sumonta Kumar Paul[1], Keisuke Yuasa[1], Masako Dannoura[1], Daniel Epron[1]

[1] Graduate School of Agriculture, Kyoto University, 606-8502, Japan

Correspondence to: Sumonta Kumar Paul (paulsumonta@gmail.com), Daniel Epron (daniel.epron.3a@kyoto-u.ac.jp)

ORCID ID

SKP: 0009-0000-7293-7255

MD: 0000-0003-0389-871X

DE: 0000-0001-9451-3437

Abstract. Forest soils are generally considered a sink for atmospheric methane (CH_4), but their uptake rate can vary considerably in space and time. This study aimed to investigate the temporal patterns of spatially distributed soil CH_4 fluxes in a topographically complex cold-temperate mountain forest in central Japan. Soil CH_4 fluxes were measured nine times during the snow-free season at multiple locations within a 40-ha area in a forested watershed. A machine-learning approach was developed to upscale measured upland fluxes to the landscape scale, using topographic attributes derived from a digital elevation model and vegetation types. Upland soils were a sink of CH_4, while small wetland patches emitted CH_4 consistently throughout the study period. The accuracy of predicted upland fluxes varied seasonally, with the highest model performance observed in early autumn (R^2 = 0.67) and the lowest in mid-summer (R^2 = 0.28). Within the study landscape, predicted upland CH_4 fluxes varied significantly across topographic positions, with greater uptake on ridges and slopes than on the plain and foot slopes. Predicted upland CH_4 fluxes ranged from -0.35 to -0.60 g CH_4 ha^{-1} h^{-1} in spring, -0.41 to -1.25 g CH_4 ha^{-1} h^{-1} in summer, and -0.50 to -0.89 g CH_4 ha^{-1} h^{-1} in autumn. Seasonal upland fluxes were highly correlated with the 20-day antecedent precipitation index (R^2 = 0.71), revealing the importance of seasonal moisture conditions in regulating CH_4 flux dynamics. This study highlighted the importance of topography in controlling the soil CH_4 fluxes and the efficiency of remote sensing and machine learning approaches in scaling field measurements to the landscape level, enabling visualization of spatial patterns of fluxes across the landscape over time.

1 Introduction

Methane (CH_4), the second most important anthropogenic greenhouse gas, contributes substantially to the anthropogenic radiative forcing and is responsible for approximately 0.5°C of current global warming compared to 1850 - 1900 (IPCC, 2023). Natural wetlands (149 Tg CH_4 yr^{-1}) and rice cultivation (30 Tg CH_4 yr^{-1}) are important sources of CH_4; in contrast, upland soils are considered a biological sink of atmospheric CH_4, with an estimated uptake of 25-45 Tg yr^{-1}, contributing 5-7% to the global CH_4 sink (Saunois et al., 2020). Among the upland ecosystems, forest soils account for approximately 60% of global soil CH_4 uptake (Dutaur and Verchot, 2007), and soil uptake rates are particularly high in Japanese mountainous forests due to their high porosity (Ishizuka et al., 2000). CH_4 uptake by forest soils is driven by methane-oxidizing bacteria in oxic soil layers,

https://doi.org/10.5194/egusphere-2025-3449
Preprint. Discussion started: 8 August 2025

whereas anaerobic environments such as wetland soils are usually dominated by methanogenic archaea producing CH_4 (Christiansen et al., 2016). CH_4 production can also occur in upland soils, either in deeper soil layers or in microsites located in otherwise well-aerated soil layers, if anaerobic conditions prevail (Angel et al., 2012). Hence, CH_4 oxidation and production can occur simultaneously at the same location, determining the net flux.

Net soil CH_4 fluxes depend mainly on the soil air-filled porosity (AFP), which in turn depends on total porosity and soil water content. A high AFP enhances gas diffusion in soil and, consequently, microbial CH_4 oxidation (Kruse et al., 1996). Soil organic matter at the soil surface can act as a physical barrier to atmospheric CH_4 diffusion and reduce the CH_4 uptake rate (Yu et al., 2017). Conversely, carbon substrates released by the decomposition of soil organic matter can increase CH_4 oxidation activity either by directly stimulating the growth of methanotrophs or by promoting CH_4 production in anaerobic microsites and indirectly supporting the growth of methanotrophs (West and Schmidt, 1999). Additionally, soil nutrients can influence soil CH_4 fluxes by regulating the soil microbial community. The activity of methanotrophic microorganisms is affected by the availability of inorganic nitrogen (Bodelier and Laanbroek, 2004). Although methanotrophic activity can be nitrogen-limited in forest soils (Veldkamp et al., 2013), increasing ammonium (NH_4^+) concentration often reduces CH_4 uptake due to competitive inhibition by NH_4^+ of the enzyme methane mono-oxygenase, which can oxidize both CH_4 and NH_4^+. Nitrate (NO_3^-) can also be a potent inhibitor of CH_4 oxidation in some soils (Mochizuki et al., 2012). Although temperature affects microbial activities, including methanogenesis and methanotrophy (Luo et al., 2013; Praeg et al., 2017), CH_4 uptake is generally less sensitive to changes in soil temperature than in soil moisture (Epron et al., 2016).

Topography and vegetation cover can create a predictable distribution of soil moisture and nutrients across topographically complex landscapes (Jeong et al., 2017; Murphy et al., 2011). In Japan, forests cover 68% of the land, mostly in mountainous areas. Conifers account for 44% of the total forest area (Lundbäck et al., 2021; Nakamura and Krestov, 2005). Topography is a critical determinant of soil hydrological conditions, from well-drained slopes to waterlogged riparian areas (Kaiser et al., 2018). Topography can also impact soil nutrient availability by altering leaf litter accumulation and the movement of soil nutrients (Osborne et al., 2017; Tateno and Takeda, 2003). The spatial distribution of trees, differences in species abundance across the landscape, and variation in litter chemistry often create heterogeneity in soil nitrogen cycling (Osborne et al., 2017). Furthermore, differences in stem flow and throughfall related to differences in canopy structure between tree species can indirectly influence spatial patterns of soil moisture (Holwerda et al., 2006).

In situ chamber measurements have long been the dominant method for studying CH_4 fluxes in forests, providing insight into the processes that drive them (Brumme and Borken, 1999; Guckland et al., 2009; Itoh et al., 2009). Until recently, most studies reported spatially average flux values measured at several locations (Gomez et al., 2016; Itoh et al., 2009). This method is acceptable for small patches of homogeneous landscapes, such as crops or single-species tree plantations in flat terrain. However, it is inappropriate for more complex landscapes, as the number of sampling points required to obtain an accurate spatially-averaged flux would increase considerably.

In complex terrains, measurement locations can be grouped into several distinct categories according to landforms (Courtois et al., 2018; Gomez et al., 2016; Itoh et al., 2009; Kagotani et al., 2001; Kaiser et al., 2018; Warner et al., 2018), soil microtopographic features (Epron et al., 2016), vegetation characteristics (Guckland et al., 2009), or land uses (Jacinthe et al., 2015). However, as Vainio et al. (2021) pointed out, aggregation assumes spatial

https://doi.org/10.5194/egusphere-2025-3449
Preprint. Discussion started: 8 August 2025

homogeneity of fluxes within each category or requires a large number of sampling points to capture the spatial heterogeneity, and this approach ignores the spatially continuous nature of soil processes and their drivers.

More recently, regressions with multiple landscape attributes derived from remote sensing-based maps were successfully applied to upscale CH_4 to a catchment scale (Kaiser et al., 2018). Recent studies conducted on a 12-ha forested watershed (Warner et al., 2019), a 10-ha boreal forest plot (Vainio et al., 2021) , two northern peatland-forest-mosaic catchments of 4.5 km^2 and 7.9 km^2 respectively (Räsänen et al., 2021), and a 450-ha subarctic tundra (Virkkala et al., 2024) have demonstrated the effectiveness of machine-learning modeling approaches for upscaling CH_4 fluxes from remote sensing data.

This study aimed to assess temporal variations of soil CH_4 fluxes across a topographically complex landscape in a cold-temperate mountain forest in central Japan and to estimate soil CH_4 fluxes at the landscape scale. We measured soil CH_4 fluxes several times during the snow-free season at multiple locations within a 40-ha area in a forested watershed. We applied a random forest machine-learning approach in combination with terrain attributes from remotely sensed data, i.e., a digital elevation model (DEM), to upscale measured soil CH_4 fluxes to the landscape level. We hypothesized that (1) terrain attributes related to water accumulation are reliable predictors of soil CH_4 fluxes, (2) predicted soil CH_4 fluxes vary within the landscape depending on topography (3) spatial patterns of uncertainties in predicted soil CH_4 fluxes vary seasonally due to a wet early summer influenced by the East Asian monsoon, and (4) seasonal variations of CH_4 flux at the landscape scale are explained by recent past precipitations.

2 Materials and methods

2.1 Description of the study site and experimental design

This study was conducted in the forested upper Yura River watershed (35.34 N; 135.76 E) located at the Ashiu Experimental Forest of Kyoto University in northeastern Kyoto Prefecture, Japan (Fig. 1). The mean annual temperature and precipitation were 10.3°C and 2,732 mm, respectively, between 2011 and 2020 and the ground was covered by snow (2-3 m depth) from mid-December to mid-April (Epron et al., 2023). The study area is characterized by a cool-temperate monsoon climate, with a very humid early summer (520 mm in June and July on average between 2011 and 2020) and occasionally heavy precipitation caused by typhoons in late summer. The soils in the study area are classified as brown forest soils according to the Classification of Forest Soils in Japan, with a relatively thick brownish-black A horizon with a crumb structure and a brown B horizon with a blocky structure (Hirai et al., 1988; Ueda et al., 1993). The forest is primarily dominated by *Cryptomeria japonica* D. Don (Japanese cedar, 73% of the basal area in four 1-ha census plots), mixed with more than 50 broadleaved species (Ishihara et al., 2011).

https://doi.org/10.5194/egusphere-2025-3449
Preprint. Discussion started: 8 August 2025

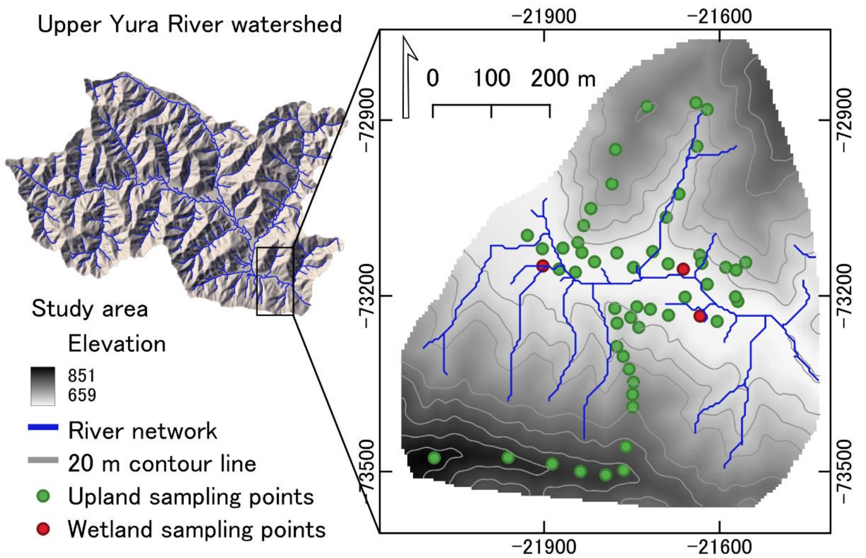

Figure 1: Map of the upper Yura River watershed with an enlargement of the 40.2 ha study area. The green dots represent the 52 flux measurement locations on unsaturated soils (upland) and the red dots the 3 measurement locations on waterlogged wetlands.

The study site covered an area of 40.2 hectares (Fig. 1) and included a variety of landscapes, ranging from ridges to waterlogged wetlands. It has a mountainous topography with an elevation between 650 and 850 m and slopes that vary from gentle to steep. The site was classified into uplands (including ridges, slopes, foot slopes and plains as topographic positions where the soil is almost always unsaturated), wetlands (small patches with water-saturated soil in the valley), and rivers, accounting for approximately 94%, 1%, and 5% of the total study area, respectively. Soil CH_4 fluxes were measured on 52 sampling points in upland areas, distributed across the four topographic positions, to optimize the representation of topographic and vegetation variations that can influence soil properties and, consequently, soil CH_4 fluxes. We also measured soil CH_4 fluxes in three small wetland patches (one sampling point in each). Unfortunately, the machine learning model we developed (see below) was unable to accurately predict fluxes across the landscape when wetland measurements were included in the training dataset. We recorded the positions of all sampling locations using a portable GPS tracker (Garmin, eTrex® Touch 35) with an accuracy of less than 5 m.

2.2 Flux measurements

Soil CH_4 fluxes were measured using a static, non-steady-state, non-flow-through system composed of a dark acrylic chamber (20 cm diameter and 12.5 cm height) connected to a cavity-enhanced absorption spectroscopy gas analyzer (Li 7810, Licor; Lincoln, USA) with two PTFE tubes, each 1.8 m long and 4 mm in inner diameter. One week before the first measurements, a 20 cm diameter, 9 cm tall PVC collar was inserted approximately 5 cm into the soil at each of the sampling point. Flux from each collar was measured on nine occasions in 2023: in

https://doi.org/10.5194/egusphere-2025-3449
Preprint. Discussion started: 8 August 2025

early spring after snowmelt (4/27), mid-spring (5/12), late spring (5/31), early summer (7/06), mid-summer (7/26), late summer (9/04), early autumn (10/07), mid-autumn (11/07), and late autumn (11/30).

To measure soil CH_4 flux, the chamber was placed on the collar, and changes in CH_4 and CO_2 concentrations inside were recorded for 4 minutes at a frequency of 1 Hz. The slope of the linear regression of CH_4 concentration over time was used to calculate the soil CH_4 flux:

$$F_{CH_4} = \frac{\Delta[CH_4]}{\Delta t} \times \frac{V \times P}{A \times R \times T}$$

where F_{CH_4} is the soil CH_4 flux, $\frac{\Delta[CH_4]}{\Delta t}$ is the slope of the linear change in CH_4 concentrations over time, V is the system volume (chamber, collar above the ground, tubes, and analyzer), A is the soil area covered by the collar, and R is the ideal gas constant (8.314 J K^{-1} mol^{-1}). A constant value of 93,525 Pa for an elevation of 650 m was used for the atmospheric pressure (P). The slope was calculated over 90 seconds following Epron et al. (2023). The R^2 of the linear variation of CH_4 concentration was less than 0.9 for a single measurement, and for this measurement, the R^2 of the linear variation of CO_2 concentration was 0.99, indicating that the low R^2 for CH_4 was due to the near-zero CH_4 flux and not to an erroneous measurement.

2.3 Topographic characterization

To characterize and process the terrain attributes related to soil CH_4 fluxes, we used a 0.5 m mesh digital elevation model (DEM) based on airborne laser surveys conducted throughout the upper Yura River watershed in 2012 by the Ashiu Experimental Forest staff. The DEM was further processed and conditioned into a 5 m mesh DEM image according to the GPS tracker's accuracy (less than ≤ 5 m) that was used to locate each collar position, enabling us to identify the corresponding pixels on the terrain attribute grids. We derived several topographic attributes from the DEM using SAGA Next Generation in QGIS (v3.34.5-Prizren). The calculated attributes included aspect, slope, profile curvature (PrC), topographic position index (TPI), topographic wetness index (TWI), and vertical distance to channel network (VDCN). Slope and TPI were used to partition the landscape into ridges, slopes, foot slopes and the plain.

Aspect, slope, and profile curvature were calculated following the 9-parameter 2nd order polynom method (Zevenbergen and Thorne, 1987). Aspect, a circular variable, was transformed into a linear variable by calculating the cosine of the aspect values, resulting in a range from -1 (south) to 1 (north). Negative values of profile curvature indicate a convex surface where the flow of water accelerates as it moves downslope; in contrast, positive values suggest a concave surface where the flow slows down (Pachepsky et al., 2001).

TWI was calculated using the equation $TWI = \ln(CA/slope)$, where CA refers to the catchment area. We derived CA from a filled DEM using the multiple flow direction algorithm (Freeman, 1991; Wang and Liu, 2006). A filled DEM is a hydrologically corrected elevation model in which erroneous surface depressions have been removed to avoid biases in water accumulation and flow direction.

TPI describes the relative position of a location within a landscape, indicating whether it is on a ridge, slope, or valley based on the elevation compared to the surrounding terrain at a specified radius (Ågren et al., 2014). Positive values indicate ridges; negative values indicate depressions, and zero or near-zero values indicate slopes or flat areas. TPI was calculated at the center of circular areas of 30 m radius using the unfilled DEM.

VDCN was calculated as the elevation difference between each grid cell and the baseline of the nearest stream channel. This parameter serves as a proxy for groundwater depth, with lower VDCN values typically corresponding to areas with shallower groundwater and higher water tables, and higher values indicating deeper groundwater levels often found in upland positions (Bock and Köthe, 2008).

2.4 Vegetation classification

Tree inventory was conducted during the flux measurement period to classify the vegetation surrounding the flux measurement points. A circular plot with a 10-meter radius was established, centered at each flux measurement point. Within the plot, all trees were identified at the species level, and their diameter at breast height (DBH) was measured. Vegetation types were classified based on the proportional contribution of coniferous and broadleaved trees to the plot basal area, the sum of cross-sectional areas at breast height of all tree trunks in each plot. Three types were defined: coniferous when the proportional contribution of coniferous trees was higher than 0.75, broadleaf when it was lower than 0.25, or mixed (comprising both coniferous and broadleaf).

2.5 Soil sampling and analysis

After completing the flux measurements, soil cores were collected using a sampling cylinder at 0-10 cm depth near the flux measurement points. Samples were sieved at 2 mm and separated into stones and fine earth. The fresh weight of the fine earth fraction was measured before being air-dried. Bulk density of this fraction was determined as the ratio of oven-dried soil (subsample dried at 105°C) to the soil volume. Soil texture was analyzed using the micro-pipette method, following Burt et al. (1993). Total soil carbon (C) and nitrogen (N) contents were measured using a Macro Corder JM 1000CN (J-SCIENCE LAB Co., Ltd., Japan). The soil pH was measured in a suspension (10 g of soil in 25 ml distilled H2O) after shaking for 1 hour.

2.6 Climatic data

Air temperature and rainfall were measured every 10 minutes at a nearby weather station operated by the Field Science Education and Research Centre of Kyoto University. The antecedent precipitation index (API), an indicator of soil moisture conditions, was calculated using the following equation:

$$\mathrm{API}_n = \sum_{t=1}^{n} P_t \times k^t$$

where, Pt is the precipitation during day t, k is the recession coefficient, and n is the number of antecedent days. The parameter k accounts for the water removed from the soil by evapotranspiration and drainage.

2.7 Modeling

In this study, modeling was conducted independently for each of the nine measurement dates. We applied quantile regression forests (QRF) introduced by Meinshausen (2006), an extension of the random forests (RF) algorithm. RF is an ensemble learning method that builds a set of regression trees, and the final prediction is the average of all the regression trees, which are evaluated using out-of-bag cross-validation (Breiman, 2001). The QRF algorithm estimates the full conditional distribution of the response variable as a function of its predictors, not just the mean as with the original RF algorithm. Therefore, it is possible to extract the prediction interval for each pixel across the landscape for each measurement period. We followed three steps to develop models for predicting soil CH_4 fluxes at each measurement period. We used the six topographic features (aspect, slope, PrC, TPI, TWI, and VDCN) and the three vegetation types listed above as predictors. Before applying QRFs, we eliminated the less important variables and identified the most relevant predictors for each measurement date, using a variable

https://doi.org/10.5194/egusphere-2025-3449
Preprint. Discussion started: 8 August 2025

selection algorithm for random forest models proposed by Genuer et al. (2010) and implemented in the "VSURF" package for R (Genuer et al., 2015). This approach systematically uses a repeated cross-validation procedure to rank variables by their importance index and iteratively eliminates the least informative ones to minimize model error. The result is a refined subset of predictors that enhances model interpretation and predictive performance. This predictor reduction approach has been previously used for mapping CH_4 fluxes (Räsänen et al., 2021; Warner et al., 2019) and soil properties (Jeong et al., 2017; Miller et al., 2015).

After selecting the relevant predictor variables, the QRF models were trained to predict CH_4 fluxes for each of the nine measurement dates using the R-packages "caret" (Kuhn and Johnson, 2013) and "quantregForest" (Meinshausen, 2017). The mtry parameter, which determines the number of randomly selected predictor variables at each node, was tested from 2 to n-1 (n being the total number of predictors) using leave-one-out cross-validation to minimize prediction error and maximize the variance explained by the model. The ntree parameter was set to 500, ensuring the model constructed an ensemble of 500 decision trees. Furthermore, we calculated the variable's importance scores using the "vip" R-package (Greenwell and Boehmke, 2020). For each of the nine measurement dates, model accuracy was evaluated based on the root mean square error (RMSE) and coefficient of determination (R^2). The output of the QRF was a set of conditional prediction distributions of CH_4 fluxes for each landscape pixel and measurement dates. Because these prediction distributions were often not normally distributed, the medians of the conditional prediction distributions at each pixel were used as the final predictions, and the interquartile ranges of these distributions were used to quantify the uncertainty in the predictions (Warner et al., 2019). Prediction uncertainties were expressed as a percentage (i.e., interquartile range of the conditional prediction distribution divided by the median).

2.8 Statistical analysis

We used analysis of variance (ANOVA) to test the differences in soil properties across the topographic positions and vegetation types. A linear mixed-effect model (LMM) was used to test the effects of topographic positions, vegetation types, and measurement dates (fixed effects) on measured CH_4 fluxes, where sampling points (collar ID) were included as a random effect. Similarly, LMM was used to test the relationship between the predicted and measured fluxes (fixed effect), with flux measurement dates as a random effect. The root mean square error (RMSE) was used to evaluate model performance at each date, and the marginal and conditional coefficients of the determinant (R_m^2 and R_c^2) were used to determine the strength of the relationship between the predicted and measured fluxes. LMM was carried out using the 'lmerTest' package (Bates et al., 2015; Kuznetsova et al., 2017), and R_m^2 and R_c^2 were calculated using the 'MUMIn' package (Bartoń, 2010). To test the effects of topographic positions and measurement dates on predicted CH_4 fluxes while accounting for spatial autocorrelation, we also used a linear mixed-effect model. Topographic positions and measurement dates were included in the model as fixed effects, and pixel ID as a random effect. To eliminate spatial autocorrelation among residuals, we incorporated an exponential spatial correlation structure based on each pixel coordinate nested within each measurement date. This was performed using the 'nlme' package (Pinheiro et al., 1999). The semi-variogram of the residuals confirmed that the residuals were not spatially correlated. A pairwise comparison across the topographic positions within each measurement date was performed using the 'emmeans' package (Lenth, 2017). Linear regression models were used to examine the relationship between scaled soil CH_4 fluxes and API. The recession coefficient (k) and the number of antecedent days (n) were not fixed a priori but optimized to maximize R^2 while ensuring the best distribution of the residuals, allowing parameters k and n to vary iteratively from 0.6

https://doi.org/10.5194/egusphere-2025-3449
Preprint. Discussion started: 8 August 2025

to 0.9 with an increment of 0.01 and from 0 to 30 with an increment of 0.01, respectively. Using a more complex bivariate model with an exponential function of air temperature did not improve the quality of the fit and returned Q_{10} values that were not significantly different from 1, as previously reported (Epron et al., 2016). Calculations, modelling, and statistical analyses were performed using the R statistical programming environment (R Core Team, 2024).

3 Results

3.1 Variations in soil properties, vegetation, and methane fluxes across the landscape

Topographic positions influenced several soil properties, whereas vegetation type and its interaction with positions had no significant effects (Table 1). Overall, the bulk density of the fine earth fraction was relatively low due to the presence of stones, highest in the plain (0.48 ± 0.05 g cm^{-3}, mean ± SE and significantly lowest in the ridge (0.26 ± 0.04 g cm^{-3}). Soil pH differed significantly across topographic positions ($p < 0.001$), with more acidic conditions observed at higher elevations (ridge: 4.0 ± 0.14) compared to the plain (5.0 ± 0.12). Similarly, total carbon (C) and total nitrogen contents (N) were significantly higher on the ridges (16.7 ± 2.2% C and 0.8 ± 0.10% N) and lower in the plain (3.9 ± 0.60% C and 0.3 ± 0.04% N).

In contrast, the soil texture of the fine earth fraction (clay, silt, and sand) did not vary significantly with topographic positions. Vegetation types varied depending on topographic positions, where broadleaved species dominated in the lower positions (77.8% in the plain and 56.3% in foot slopes), while conifers and their mixtures with broadleaved species dominated the ridges and slopes (Table A1).

We observed that upland soils consistently uptake CH_4 (negative fluxes, Fig. 2a, b), while soils in the three small wetland patches emitted CH_4 (positive flux, Fig. A1). In the upland areas, the linear mixed-effect model (LMM) indicated that topographic positions ($p = 0.17$) and vegetation types ($p = 0.83$) individually had no significant effects on soil CH_4 fluxes (Fig. 2a, b; Table A2). However, all upland topographic positions and vegetation types showed the same distinct significant variation in CH_4 fluxes across the measurement dates ($p < 0.001$), which was consistent with the seasonal patterns of rainfall and air temperature (Fig. 2; Table A2). Although two-way interactions among positions, vegetation types, and measurement dates were not significant, their three-way interaction was (Table A2). We also found that mean CH_4 fluxes from upland areas were significantly correlated with soil pH ($r = 0.32$; $p < 0.05$, Table A3), while they were not significantly correlated with soil C, N, or bulk density.

https://doi.org/10.5194/egusphere-2025-3449
Preprint. Discussion started: 8 August 2025

Table 1. Soil physical and chemical properties (mean ± standard error) according to topographic positions and vegetation types. Different lowercase letters indicate significant differences between topographic positions and vegetation types ($p < 0.05$). The p-values from two-way ANOVA are shown in the last rows. The number of independent replicates in each factor level is indicated in the first column. Significant differences between fertilization levels are indicated by different lowercase letters.

Factors	Bulk density (g cm^{-3})	Clay %	Silt %	Sand %	pH	Total carbon (%)	Total nitrogen (%)
Position:							
Plain (n = 9)	0.48 ± 0.05 a	10 ± 2	28 ± 3	63 ± 5	5.0 ± 0.12 a	3.9 ± 0.60 a	0.3 ± 0.04 a
Foot slope (n = 16)	0.34 ± 0.04 ab	9 ± 2	31 ± 3	60 ± 5	4.5 ± 0.08 b	7.9 ± 0.98 ab	0.5 ± 0.05 a
Slope (n = 14)	0.28 ± 0.03 b	9 ± 1	28 ± 2	63 ± 3	4.3 ± 0.06 bc	10.4 ± 1.50 b	0.6 ± 0.08 ab
Ridge (n = 13)	0.26 ± 0.04 b	9 ± 2	23 ± 4	68 ± 4	4.0 ± 0.14 c	16.7 ± 2.2 c	0.8 ± 0.10 b
Vegetation:							
Broadleaved (n = 19)	0.38 ± 0.04	10 ± 2	29 ± 3	61 ± 4	4.7 ± 0.10	6.8 ± 0.98	0.4 ± 0.05
Coniferous (n = 11)	0.32 ± 0.04	7 ± 1	27 ± 4	66 ± 5	4.3 ± 0.13	11.1 ± 2.37	0.6 ± 0.11
Mixed (n = 22)	0.28 ± 0.03	9 ± 1	26 ± 2	64 ± 3	4.2 ± 0.09	12.4 ± 1.59	0.6 ± 0.07
ANOVA results:							
Position	p < 0.01	p = 0.97	p = 0.43	p = 0.6	p < 0.001	p < 0.001	p < 0.01
Vegetation	p = 0.93	p = 0.37	p = 0.99	p = 0.89	p = 0.89	p = 0.97	p = 0.95
Position × Vegetation	p = 0.45	p = 0.51	p = 0.29	p = 0.21	p =0.72	p = 0.68	p = 0.59

https://doi.org/10.5194/egusphere-2025-3449
Preprint. Discussion started: 8 August 2025

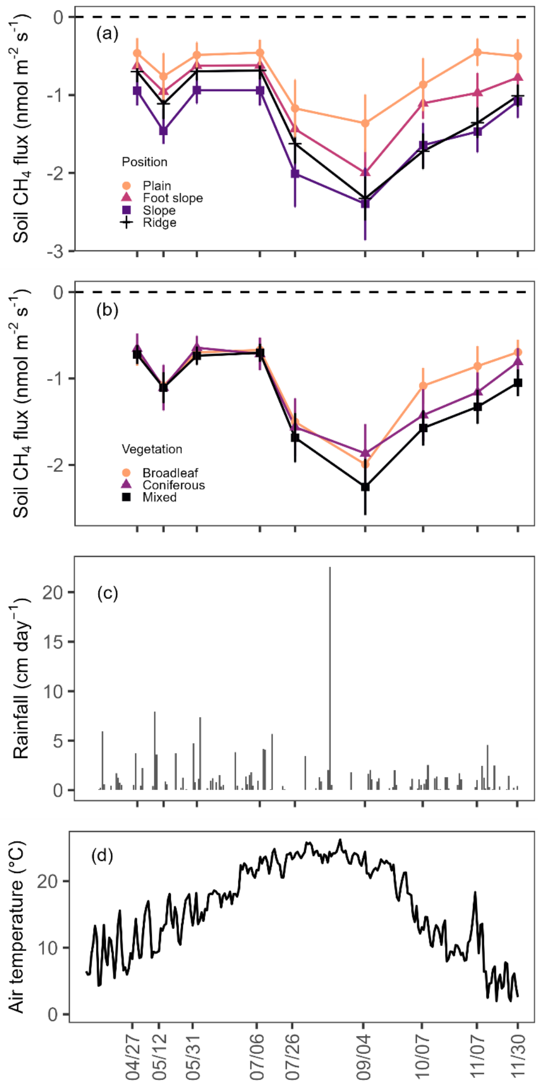

Figure 2: Seasonal variations in soil CH_4 fluxes (mean ± standard error) according to (a) topographic positions (n = 9 for the plain, 16 for foot slopes, 14 for slopes, and 13 for ridges), (b) vegetation types for upland measurement locations (n = 19 for broadleaved, 11 for coniferous, and 22 for mixed), (c) daily precipitation, and (d) daily mean air temperature from April to November in 2023.

3.2 Selected variables and performance of the upland CH_4 flux models

The topographic position index (TPI) was consistently selected in all seasons, with high importance scores, ranging from 0.51 to 0.90, depending on the measurement dates (Table 2). The topographic wetness index (TWI) was selected for most measurement dates, except two, where the vertical distance to the channel network (VDCN) was selected instead. TWI importance scores were high in early spring (0.64), late spring (0.61), and mid-summer

https://doi.org/10.5194/egusphere-2025-3449
Preprint. Discussion started: 8 August 2025

(0.63). VDCN and profile curvature (PrC) were occasionally selected along with TPI and TWI. VDCN showed moderate importance scores, contributing mostly in mid-spring (0.67) and early autumn (0.57). PrC, although less consistently selected, played a role in specific seasons, particularly early spring (0.55) and mid-autumn (0.51). Vegetation type was never selected in any season.

Table 2. Selected variables for each measurement date, along with the R^2 and root mean square error (RMSE) values to evaluate the accuracy of the quantile regression forests (QRFs) model. Importance scores of the selected variables are shown in parentheses, indicating their contribution to predicting soil CH_4 fluxes.

Measurement dates	Selected variables	R^2	RMSE (nmol m^{-2} s^{-1})
2023/04/27	TWI (0.64), TPI (0.63), PrC (0.55)	0.48	0.53
2023/05/12	TPI (0.80), VDCN (0.67)	0.31	0.82
2023/05/31	TWI (0.61), TPI (0.54), VDCN (0.53)	0.46	0.47
2023/07/06	TWI (0.52), TPI (0.58)	0.28	0.51
2023/07/26	TWI (0.63), TPI (0.57), VDCN (0.47)	0.30	1.07
2023/09/04	TWI (0.51), TPI (0.71), VDCN (0.35)	0.43	1.15
2023/10/07	TPI (0.87), VDCN (0.57)	0.67	0.81
2023/11/07	TWI (0.24), TPI (0.90), PrC (0.51)	0.61	0.68
2023/11/30	TWI (0.49), TPI (0.52), VDCN (0.41)	0.44	0.57

Model accuracy showed seasonal variation, with the highest obtained in early autumn (R^2 = 0.67; RMSE = 0.81 nmol m^{-2} s^{-1}) and the lowest in early wet summer (R^2 = 0.28; RMSE = 0.51 nmol m^{-2} s^{-1}; Table 2). The relationship between measured and predicted fluxes for each measurement date showed that estimated fluxes were close to the observed fluxes (Fig. 3a-i).

https://doi.org/10.5194/egusphere-2025-3449
Preprint. Discussion started: 8 August 2025

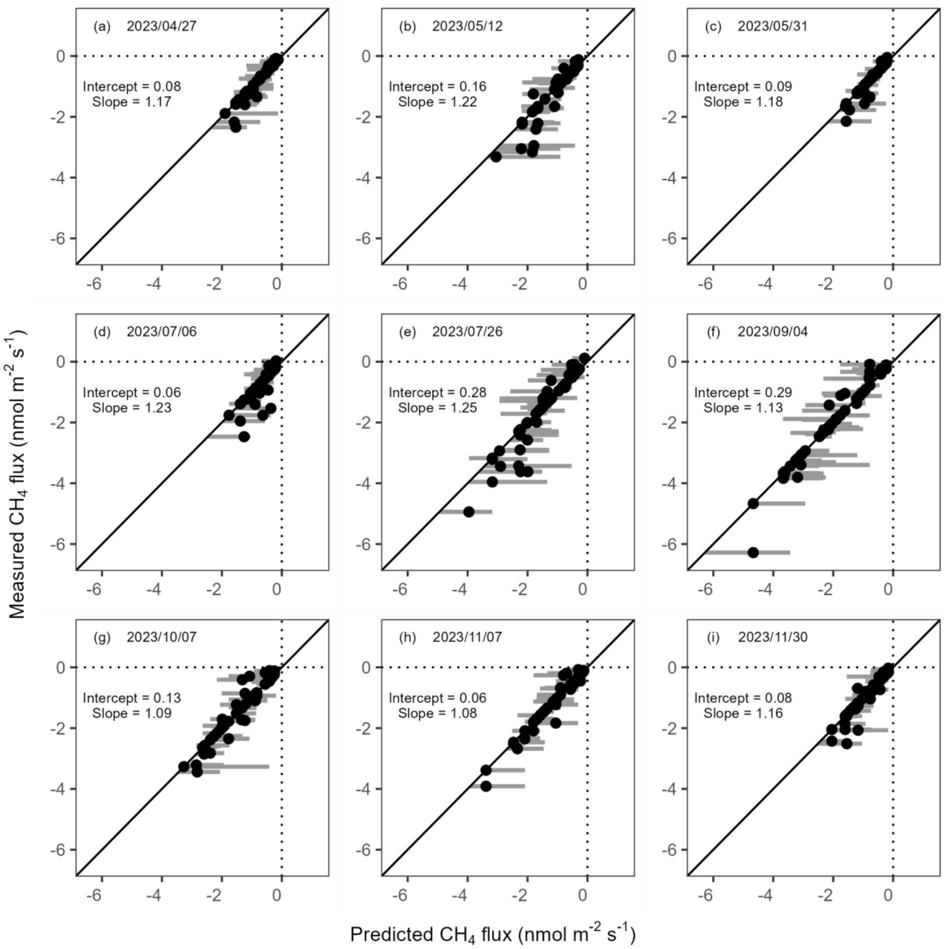

Figure 3: Comparison of predicted (median of the quartile predictions from QRFs) and measured CH_4 fluxes for each measurement date. Vertical bars indicate the interquartile ranges of the prediction distribution. Intercepts and slopes are estimated using a linear mixed-effect model with measurement dates as a random effect (full statistics are shown in Table A4).

Overall, the slope of the relationship between measured and predicted fluxes (fixed effects) was not significantly different from 1 and was similar at all dates. The marginal (R^2_m) and conditional (R^2_c) coefficients of determination were 0.93 and 0.94, respectively, highlighting the consistency of the prediction for all measurement dates (linear mixed model, Table A4).

3.3 Predicted upland soil CH_4 fluxes

Predicted median CH_4 fluxes showed significant spatial heterogeneity and temporal variability across the landscape (Fig. 4; Table A6).

https://doi.org/10.5194/egusphere-2025-3449
Preprint. Discussion started: 8 August 2025

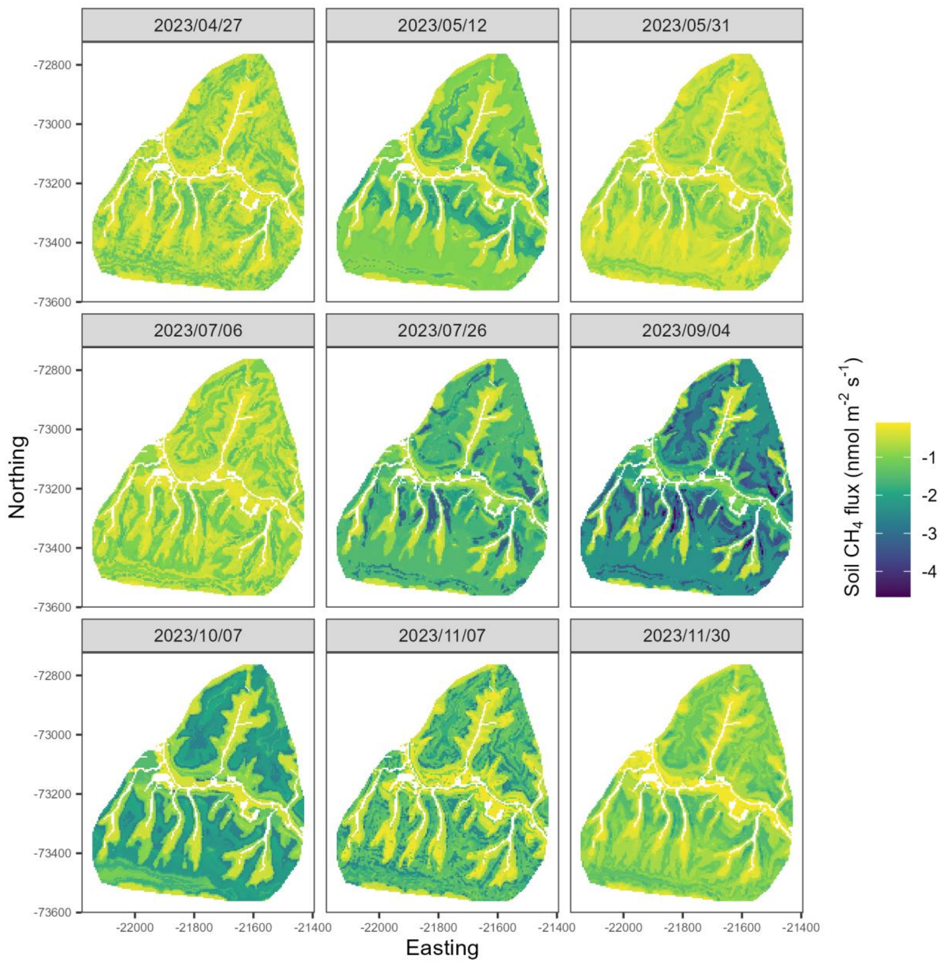

Figure 4: Maps of predicted soil CH_4 fluxes at each pixel of the study area for each measurement date. Values represent the median of the conditional prediction distribution for each pixel.

Spatial trends were consistent across seasons, with the highest net CH_4 uptake observed on ridges and steepest parts of the slopes and decreasing toward the foot slopes near streams and the flat plain (Fig. 5; Table A6).

In early (April 27) and late spring (May 31), CH_4 uptake was low across the landscape. Higher uptake was predicted in mid-spring (May 12), consistent with measurements when there was less rain and warmer temperatures. CH_4 uptake was still low in the early wet summer (July 6) and increased toward the mid to late dry summer (July 26 and Sep 4). Net CH_4 uptake then decreased from early autumn (Oct 7) and reached its lowest rate in late autumn (Nov 30).

https://doi.org/10.5194/egusphere-2025-3449
Preprint. Discussion started: 8 August 2025

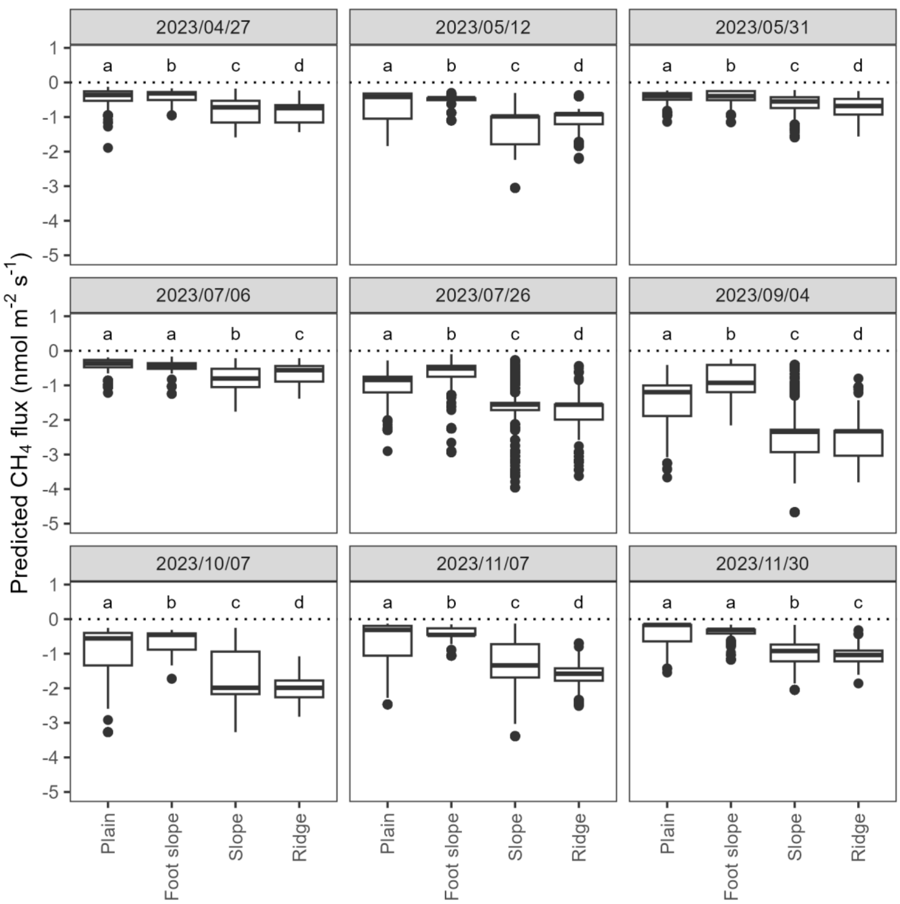

Figure 5: Predicted landscape-scale soil CH_4 fluxes for each measurement date at the pixel level, aggregated by upland topographic positions. Different letters indicate significant differences between topographic positions for each measurement date.

3.4 Uncertainty of predicted upland soil CH_4 fluxes

The spatial distribution of the percentage of predicted uncertainty varied across seasons (Fig. 6). The percentage was consistently low to moderate (less than 100%) for pixels on ridges and steep slopes, but extremely high uncertainties (more than 500%) was observed at some dates for low-elevation pixels when predicted fluxes were close to zero. However, low predicted fluxes were often associated with equally low predicted uncertainty (Fig. 6, A2). The proportion of pixels with low uncertainty (<50%) was highest in early autumn (39.7% of the total upland pixels) and lowest in early spring (4.5% of the total upland pixels). In contrast, moderate uncertainty (50-100%) was predominant in most seasons, particularly in spring and autumn, accounting for approximately 50% of the landscape. Moderate to high uncertainty (101-500%) was also predominant at some measurement dates, reaching its highest contribution of the landscape in late spring (47.6%). Extreme uncertainty (>500%) was very rare in all seasons, generally below 0.2%, except for a small peak in late autumn (0.5%) (Table A7).

https://doi.org/10.5194/egusphere-2025-3449
Preprint. Discussion started: 8 August 2025

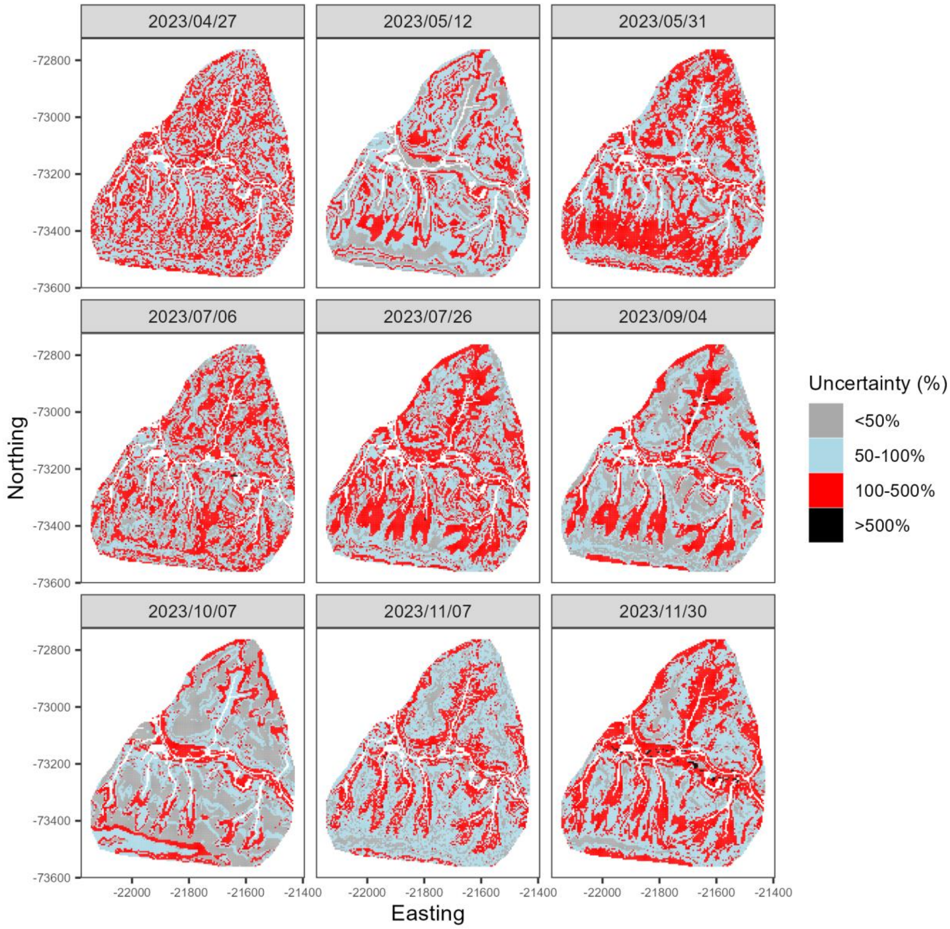

Figure 6. Uncertainty map of predicted soil CH_4 fluxes at each pixel of the study area for each measurement date. Values represent the ratio of the interquartile range to the median of the prediction distribution for each pixel.

350

3.5 Predicted seasonal upland fluxes at the landscape level

The predicted upland CH_4 flux per hectare was calculated as the sum of the predicted fluxes at each pixel multiplied by pixel area (25 m^2), and the sum divided by the upland area. Across the landscape, predicted median seasonal fluxes ranged from -0.35 to -0.60 g CH_4 ha^{-1} hr^{-1} in spring, from -0.41 to -1.25 g CH_4 ha^{-1} hr^{-1} in summer,
355 and from -0.50 to -0.89 g CH_4 ha^{-1} hr^{-1} in autumn (Fig. 7a).

https://doi.org/10.5194/egusphere-2025-3449
Preprint. Discussion started: 8 August 2025

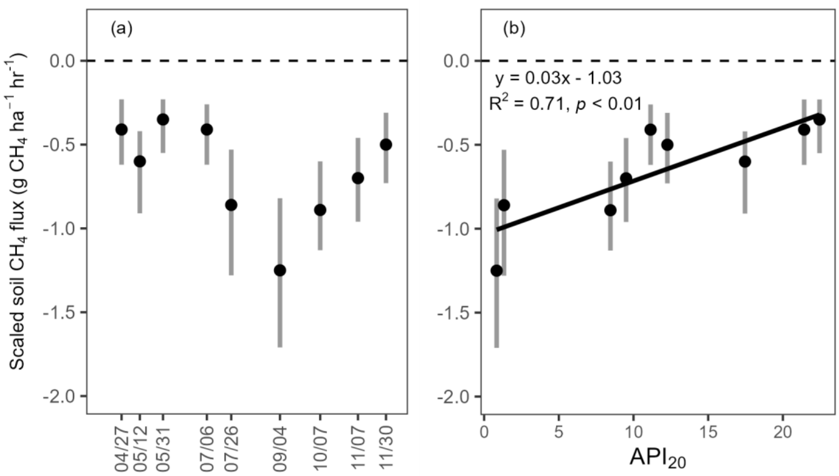

Figure 7: Predicted soil CH_4 fluxes, calculated as the mean of all pixels in the study area, and antecedent precipitation index (API). (a) Seasonal variations in landscape-scaled soil CH_4 fluxes and (b) relationship between landscape-scaled soil CH_4 fluxes and the 20-day API. Vertical bars indicate the uncertainty of the predicted fluxes.

This seasonal variation in predicted upland median fluxes was well explained by the 20-day antecedent precipitation index ($R^2 = 0.71$, $p < 0.01$) with a recession coefficient of 0.71 (Fig. 7b), followed closely by the 30-day ($R^2 = 0.70$) and 7-day ($R^2 = 0.69$) API (Table A8). The average CH_4 uptake by upland soils during the snow-free season was -0.67 (interquartile range: -0.94 to -0.43) g CH_4 ha^{-1} hr^{-1}.

4. Discussion

4.1 Selected variables

We employed quantile regression forest (QRF) models, driven by topographic and vegetation attributes, to upscale *in-situ* soil CH_4 flux measurements from sampling points to the landscape level for each measurement date in all upland topographic positions, but excluding wetlands (1% of our study area). This non-parametric machine learning approach is particularly suited for handling non-linear relationships and complex interactions among predictors (Meinshausen, 2006).

Unexpectedly, vegetation type was never selected despite previous evidence of greater soil CH_4 uptake in plots containing only deciduous broadleaved tree species than in plots containing evergreen coniferous trees, either alone or in mixture (Jevon et al., 2023). The discrepancy between this previous study and our results may be related to the fact that their study area was ten times smaller and more topographically homogeneous than ours (4 *versus* 40 ha). Moreover, soil properties that could explain the lower rate of CH_4 oxidation in coniferous than in broadleaved stands, such as higher acidity (Borken et al., 2003; Hütsch, 1998; Ishizuka et al., 2000) did not differ significantly among the three types of vegetation cover at our site, whereas they differed according to topographic position. Furthermore, vegetation types were not randomly distributed among topographic positions (Table A1), meaning that the confounding effects of vegetation and DEM-derived variables on the prediction soil CH_4 uptake could make it difficult to separate the influence of vegetation and topography in our complex mountain landscape. Among all tested topographic variables derived from the DEM, TWI, TPI, PrC, and VDCN were consistently

https://doi.org/10.5194/egusphere-2025-3449
Preprint. Discussion started: 8 August 2025

selected in different models across all measurement periods, emphasizing their importance in upscaling CH_4 fluxes. Overall, the results validated our first hypothesis, as the selected topographic attributes were related to water circulation and accumulation.

Among these variables, TWI represents water accumulation potential and is a common surrogate for soil moisture in mountainous regions. This key factor controls CH_4 fluxes by affecting gas diffusion and microbial activity (Kaiser et al., 2018; Vainio et al., 2021; Warner et al., 2019), as TWI integrates potential inflows and discharges through runoff and drainage (Ågren et al., 2014; Beven and Kirkby, 1979). TWI was selected in seven out of nine measurement periods but not on May 12 and October 7. These two periods correspond to transitional seasons, i.e., mid-spring and early autumn, when the landscape is generally drier, and water does not accumulate.

TPI describes the elevation of a location relative to those of the surrounding terrain within a given radius, allowing the identification of landform positions such as ridges, slopes, and valleys (Ågren et al., 2014). TPI is generally calculated using a non-filled DEM, which is also more representative of local-scale moist depression that TWI doesn't capture, as TWI is calculated using the filled DEM (Kemppinen et al., 2018). In our study, TPI was consistently selected in all measurement periods, highlighting that localized moisture, and potentially soil chemistry, are more influential parameters in controlling the CH_4 fluxes at the landscape level. Areas with negative TPI values (e.g., valleys or depressions) typically function as convergence zones, where water and nutrients accumulate due to gravitational flow and reduced drainage. In contrast, positive TPI values (e.g., ridges and convex upper slopes) are more divergent, often characterized by increased drainage and runoff, and limited water and nutrient retention.

Although PrC was significantly correlated to TPI (Table A5), it was selected twice (April 27 and Nov 7). PrC refers to the curvature of the land surface in the direction of the slope (along a flow line). It influences the acceleration or deceleration of surface and subsurface water flow (Ågren et al., 2014). Negative values (concave slopes) tend to slow water movement, promoting water and nutrient accumulation in soils. Conversely, positive values (convex slopes) accelerate flow, often reducing water retention time and lowering nutrient accumulation due to leaching or erosion. Excluding PrC from the list of available variables for selection decreased the model performance for these two dates, probably because PrC helps discriminate between plains and slopes, both of which have near-zero TPI values.

VDCN is another important variable reflecting groundwater level conditions. Lower values typically observed near stream channels with higher groundwater level (Bock and Köthe, 2008). When the landscape was drier (May 12 and October 7), and TWI was not selected, TPI and VDCN had more substantial explanatory power. VDCN was also selected several times with TWI. Interestingly, VDCN has been shown to be useful in distinguishing well-drained from poorly drained soils (Bell et al., 1992; Kravchenko et al., 2002). It may explain why, despite significant correlations between VDCN and both TPI and TWI (Table A5), excluding VDCN from the list of variables available for selection decreased model performance. This highlights that TWI and TPI alone were not sufficient to reflect local soil moisture conditions, as drainage conditions can potentially vary across the landscape, which controls soil microhabitat conditions and thus influences CH_4 fluxes.

4.2 Spatial patterns of predicted soil CH_4 fluxes

The models revealed clear spatial patterns in soil CH_4 fluxes that were consistent across measurement dates, even though the models selected different variables at each date. Predicted soil CH_4 fluxes closely matched topographic gradients, consistent with our second hypothesis. Ridges and upper slopes exhibited the highest net CH_4 uptake,

https://doi.org/10.5194/egusphere-2025-3449
Preprint. Discussion started: 8 August 2025

functioning as strong sinks for CH_4 across all seasons, whereas CH_4 uptakes were lowest in plain and foot slope positions. These topographic patterns of CH_4 uptake are consistent with previous studies. In a temperate forest in central Ontario, Canada, the highest CH_4 uptake was observed on slopes and ridges (Wang et al., 2013). Similarly, in a temperate forest in Maryland, USA, transition zones were identified as hotspots for CH_4 uptake (Warner et al., 2018). In a tropical forest in China, hillslopes exhibited the highest CH_4 uptake, while lower uptake was observed at the foot slopes and in groundwater discharge areas (Yu et al., 2021). Similarly, CH_4 uptake was greater on ridges than at valley bottoms in a subtropical forest in Puerto Rico (Quebbeman et al., 2022).

In our studied landscape, we observed lower soil bulk density on ridges and slopes than on the plain area, indicating that ridge and slope soils have higher porosity, which is consistent with higher soil CH_4 oxidation rates due to higher diffusion rates of O_2 and CH_4 from the atmosphere through soil pores (Ishizuka et al., 2009). Although we did not assess the methanotroph community structure, the greater atmospheric CH_4 uptake on slopes and ridges is consistent with the community structure observed in a subalpine forest, with type I methanotrophs dominating in riparian soils, whereas type II methanotrophs were more prevalent in upland soils (Du et al., 2015). The higher soil carbon (C) and nitrogen (N) contents observed on ridges and slopes at our site may contribute to higher soil CH_4 uptake, as soil CH_4 uptake has been found to be positively correlated with soil organic matter content in subtropical and temperate forests (Lee et al., 2023). Possible explanations are that higher soil carbon may increase the availability of labile substrates that stimulate methanotrophic activity by increasing CH_4 supply through enhanced methanogenesis in anoxic microsites or by directly providing substrate for facultative methane-oxidizing bacteria, thereby increasing their abundance (Jensen et al., 1998; Semrau et al., 2011; West and Schmidt, 1999). Soil nitrogen was probably predominantly in organic form, and therefore the soil concentration of nitrate and ammonium, known to inhibit CH_4 oxidation by methanotrophs at high concentration (King and Schnell, 1994; Mochizuki et al., 2012), likely remained low (Aronson and Helliker, 2010; Bodelier and Laanbroek, 2004). Nitrogen is an essential nutrient for the growth of methanotrophs, whose activity has been shown to be nitrogen-limited in forest soils (Börjesson and Nohrstedt, 2000; Martinson et al., 2021; Veldkamp et al., 2013). Therefore, mineralization of these low levels of organic nitrogen could alleviate the nitrogen limitation of CH_4 oxidation and partly explain the higher soil CH_4 uptake observed on ridges and slopes, where total nitrogen concentration was higher than at the foot slopes and in the plain.

4.3 Model performance and uncertainty

Soil CH_4 fluxes predicted by QRF models were close to the measured fluxes for all measurement periods (Fig. 3; Table A4), indicating that topographic attributes could be used for upscaling CH_4 fluxes in mountainous landscapes. The performance of the models developed for scaling CH_4 fluxes was comparable to previous studies using topographic data for similar purposes (Kaiser et al., 2018; Vainio et al., 2021; Virkkala et al., 2024; Warner et al., 2019). However, it is important to note that direct comparisons between studies are difficult due to variations in cross-validation approaches, as the choice of cross-validation technique can significantly influence model performance (Roberts et al., 2017).

Unfortunately, it was not possible to accurately predict CH_4 fluxes when measurements collected in wetland patches were included in the training data, probably because neither the topographic features nor the vegetation differed sufficiently between the large areas functioning as CH_4 sinks and the small wetland patches functioning as CH_4 sources in the plain area. Räsänen et al. (2021) noticed that spatial patterns of CH_4 fluxes could be accurately predicted in a northern peatland-forest-mosaic landscape when they were modeled for sinks and sources

https://doi.org/10.5194/egusphere-2025-3449
Preprint. Discussion started: 8 August 2025

separately. This separation was not possible in our study due to the low number of measurement locations in wetlands, related to their small extent (1%) in our upland-dominated landscape.

One advantage of the QRF approach is its ability to estimate prediction intervals (Meinshausen, 2006), thus offering insights into the uncertainty associated with the predicted flux value at each pixel. The spatial distribution of the uncertainty associated with the predicted soil CH_4 fluxes varied seasonally (Fig. 6; Table A7) in agreement with our third hypothesis, reflecting both spatial heterogeneity and temporal changes in model confidence. In our study, the spatial patterns of QRF-derived uncertainties were consistently related to topographic position and flux magnitude. Predictions in ridge and steep slope pixels generally exhibited low percentage uncertainties (often below 100%), likely because these well-drained upland areas were well represented in the training data and exhibited relatively stable and high CH_4 uptake across seasons. In contrast, extremely high percentage uncertainties (exceeding 500%) were observed in some low-lying pixels during specific seasons, especially where predicted CH_4 fluxes were close to zero. A crucial methodological point is that percentage uncertainty is a relative measure; even a small absolute uncertainty around a near-zero prediction can yield a very large percentage (Warner et al., 2019). Large absolute uncertainties can result from large differences in fluxes measured at locations with similar topographic characteristics. Since lower fluxes were measured in the flat plain area compared to the ridges and slopes, yet with similar variability (Fig. 2a), high relative uncertainties were often associated with this area characterized by complex hydrological conditions, which are difficult to model accurately.

Consistent with our third hypothesis, seasonal differences in the uncertainty distribution were also evident, with the lowest uncertainty in late summer and early autumn, i.e., under warm and dry conditions, indicating better model performance when hydrological conditions were less variable. In contrast, larger uncertainties were produced by the models in early spring and late autumn, as well as in late spring and early summer, when measured and predicted soil CH_4 fluxes were lowest. The East Asian monsoon flow bringing warm and humid air mass and resulting in the rainy season in late spring and early summer, as well as low evapotranspiration in early spring and late autumn, may have introduced greater variability in soil hydrology, contributing to higher uncertainties. Nevertheless, low to moderate uncertainty (<100%) was the most prevalent class across all seasons, consistently accounting for more than half the landscape—up to 80% in late summer and early autumn—while extreme uncertainties (>500%) were rare across all seasons. This suggests that the models performed well overall. Although some areas remain challenging to model, the QRF approach provides generally reliable spatial predictions of soil CH_4 fluxes with quantifiable and interpretable uncertainties.

4.4 Scaled soil CH_4 fluxes and seasonal variation

The upland CH_4 fluxes per hectare were calculated by aggregating pixel-level predictions and normalizing them to the total upland area, allowing for standardized comparison across sites, although there are still very few comparable data available, making it difficult to analyze the causes of differences across sites. Our highest CH_4 uptake in late summer was -1.25 g CH_4 ha^{-1} hr^{-1} (interquartile range -1.71 to -0.82), 2.6 times higher in absolute value than in a forested watershed in Maryland, USA (-0.47 g CH_4 ha^{-1} hr^{-1}, Warner et al. 2019), but slightly lower than in a boreal pine forest in Finland (-1.59 g CH_4 ha^{-1} hr^{-1}, Vainio et al. 2021).

Consistent with our fourth hypothesis, the seasonal variation in predicted upland CH_4 fluxes reflects strong sensitivity to soil moisture dynamics, which were effectively captured using the Antecedent Precipitation Index (API). The API, serving as a proxy for dynamic soil moisture, integrates precipitation over a defined period and includes a recession factor to account for evapotranspiration and drainage. Short durations (e.g., 7 days) reflect

https://doi.org/10.5194/egusphere-2025-3449
Preprint. Discussion started: 8 August 2025

surface moisture, while longer durations (e.g., 30 days) capture deeper soil moisture conditions (Schoener and Stone, 2020; Sidle et al., 2000; Yamao et al., 2016). Among the API durations tested, the 20-day API with a recession coefficient of 0.70 showed the highest explanatory power ($R^2 = 0.71$), although using either a 30-day or a 7-day API would provide similar goodness of fit with similar recession coefficients, indicating that soil moisture conditions across different depths had similar influence on CH_4 flux variability. The consistently low recession coefficient (Kohler and Linsley, 1951) suggested that rainwater does not accumulate in our watershed. Higher API values indicate wetter antecedent conditions, which can suppress CH_4 uptake by reducing oxygen availability and thus limiting methanotrophic activity, and by temporarily turning the subsoil condition to anoxic, promoting methane production and reducing net CH_4 uptake (Angel et al., 2012; Hu et al., 2023; Kruse et al., 1996). Conversely, drier periods with lower API values were observed in mid and late summer and earlier autumn, when soils were better aerated, creating favorable conditions for atmospheric CH_4 oxidation and leading to greater CH_4 uptake.

5 Conclusion

In conclusion, our study showed the dominant role of topography on the spatial variation of soil CH_4 fluxes in upland forest landscapes. The quantile regression forest (QRF) model successfully captured these ridge-to-plain spatial gradients in the upland area where the soil is almost always unsaturated, with strong performance. CH_4 uptake was consistently highest on ridges and slopes, where well-drained soils with lower bulk density and higher porosity supported enhanced methanotrophic activity. Furthermore, the seasonal dynamics of CH_4 uptake were well-captured by the 20-day Antecedent Precipitation Index (API), with a significant positive relationship between API and CH_4 uptake, emphasizing the sensitivity of CH_4 uptake by upland soils to seasonal fluctuations in soil moisture conditions. Our modeling approach was unable to accurately predict CH_4 fluxes when including measurements collected in three wetland patches functioning as CH_4 sources in the plain area (1% of the total landscape). The integration of terrain-based predictors and moisture history provides a reliable framework for scaling soil CH_4 fluxes across complex landscapes, highlighting the importance of considering both static (topographic) and dynamic (climatic) controls in future assessments of CH_4 flux.

https://doi.org/10.5194/egusphere-2025-3449
Preprint. Discussion started: 8 August 2025

Appendix A

Table A1. Proportion of vegetation types associated with the different topographic positions

Position	Vegetation	Proportion of vegetation type (%)
Plain	Broadleaf	77.8
	Coniferous	11.1
	Mixed	11.1
Foot slope	Broadleaf	56.3
	Coniferous	18.8
	Mixed	25.0
Slope	Broadleaf	21.4
	Coniferous	21.4
	Mixed	57.1
Ridge	Coniferous	30.8
	Mixed	69.2

Table A2. Summary of linear mixed model (LMMs) analyzing the effects of topographic position, vegetation types, date of measurement, and their interactions on measured soil CH_4 fluxes. Collar ID was included as the random effect.

Response variable	Explanatory factors (fixed effects)	p-value
Measured soil CH_4 fluxes	Position [df = 3]	0.17
	Vegetation [df = 2]	0.83
	Measurement date (DM) [df = 8]	$< 2 \times 10^{-16}$
	Position × Vegetation [df = 5]	0.93
	Position × DM [df = 24]	0.74
	Vegetation × DM [df = 16]	0.51
	Position × Vegetation × DM [df = 40]	0.04

https://doi.org/10.5194/egusphere-2025-3449
Preprint. Discussion started: 8 August 2025

Table A3. Spearman's correlation coefficients and p-values (*p > 0.05, **p > 0.01, ***p > 0.001) between soil properties and mean soil CH_4 fluxes. Non-significant coefficients are shown in gray.

	BD	Clay	Silt	Sand	pH	C%	N%
BD							
Clay	-0.23						
Silt	-0.06	0.40**					
Sand	0.14	-0.73***	-0.93***				
pH	0.47***	0.11	0.03	-0.064			
C%	-0.72***	-0.00	-0.10	0.078	-0.69***		
N%	-0.74***	0.01	-0.11	0.077	-0.65***	0.97***	
Mean CH_4 flux	0.26	-0.04	-0.11	0.105	0.32*	-0.20	-0.22

Table A4. Summary of the linear mixed model (LMMs) analyzing the relationship between the predicted soil CH_4 fluxes and measured soil CH_4 fluxes, where measurement periods were included as the random factor on both slope and intercept. The p-values of the fixed effect were for testing if the intercept was different from zero and the slope different from 1. The marginal (R^2_m) and conditional (R^2_c) coefficients of determination, and the root mean square error of the model are shown.

Fixed effect: predicted CH_4 flux			Random effects: measurement dates		
Estimate ± SE		p-values		Intercept	Slope
Intercept	0.12 ± 0.03	from 0: 0.004	2023/04/27	-0.03	0.02
Slope	1.15 ± 0.02	from 0: 2×10^{-11}	2023/05/12	0.00	0.03
		from 1: 0.91	2023/05/31	-0.03	0.02
			2023/07/06	-0.07	0.04
Statistics			2023/07/26	0.05	0.03
n	467		2023/09/04	0.09	-0.05
R^2_m	0.93		2023/10/07	0.03	-0.05
R^2_c	0.94		2023/11/07	-0.01	-0.04
RMSE	0.28		2023/11/30	-0.02	0.01

https://doi.org/10.5194/egusphere-2025-3449
Preprint. Discussion started: 8 August 2025

Table A5. Spearman's correlation coefficients and p-values (*p > 0.05, **p > 0.01, ***p > 0.001) between topographic attributes: cosine-transformed aspect, slope, profile curvature (PrC), topographic position index (TPI), topographic wetness index (TWI), and vertical distance to channel network (VDCN).

	Aspect	Slope	PrC	TPI	TWI
Aspect					
Slope	-0.04				
PrC	0.17	-0.01			
TPI	0.16	0.02	0.63^{***}		
TWI	-0.25	-0.58	-0.20	-0.57^{***}	
VDCN	-0.03	0.26	0.46^{***}	0.73^{***}	-0.53^{***}

Table A6. Summary of the LMM analyzing the effects of topographic position and measurement dates (MD) on predicted soil CH_4 fluxes. Pixel ID was included as a random effect, and spatial autocorrelation among residuals eliminated.

Response variables	Explanatory variables	p-values
Predicted median CH_4 fluxes	Position [df = 3]	< 0.001
	MD [df = 8]	< 0.001
	Position × MD [df = 24]	< 0.001

Table A7. Percentage of upland pixels in the study area distributed among four levels of predicted relative uncertainty for soil CH_4 fluxes.

	Uncertainty			
Seasons	< 50%	50 - 99 %	100 - 500%	>5 00%
2023/04/27	4.54%	53.06%	42.35%	0.04%
2023/05/12	19.93%	54.01%	26.06%	-
2023/05/31	8.28%	44.19%	47.54%	-
2023/07/06	21.68%	39.73%	38.50%	0.08%
2023/07/26	13.18%	43.75%	43.05%	0.02%
2023/09/04	30.85%	39.64%	29.35%	0.16%
2023/10/07	39.68%	38.13%	22.19%	-
2023/11/07	16.98%	54.58%	28.37%	0.07%
2023/11/30	11.29%	46.85%	41.34%	0.52%

https://doi.org/10.5194/egusphere-2025-3449
Preprint. Discussion started: 8 August 2025

Table A8. Statistics of the linear relationship between landscape-scaled soil CH_4 fluxes and antecedent precipitation indexes (API). 20 antecedent days provided the best fit. 30 and 7 antecedent days are shown as common metrics in hydrology. Adjusted recession coefficients (k) and determination coefficients (R^2) are shown.

Antecedent days	k	R^2
20	0.70	0.71
30	0.70	0.70
7	0.68	0.69

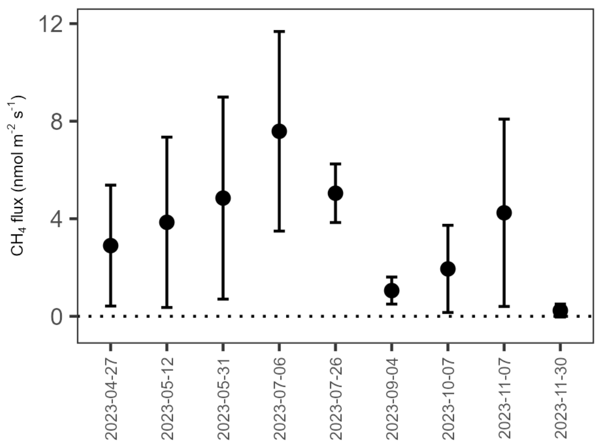

Fig A1. Seasonal variation of soil CH_4 fluxes from wetlands (means and standard error, n = 3).

https://doi.org/10.5194/egusphere-2025-3449
Preprint. Discussion started: 8 August 2025

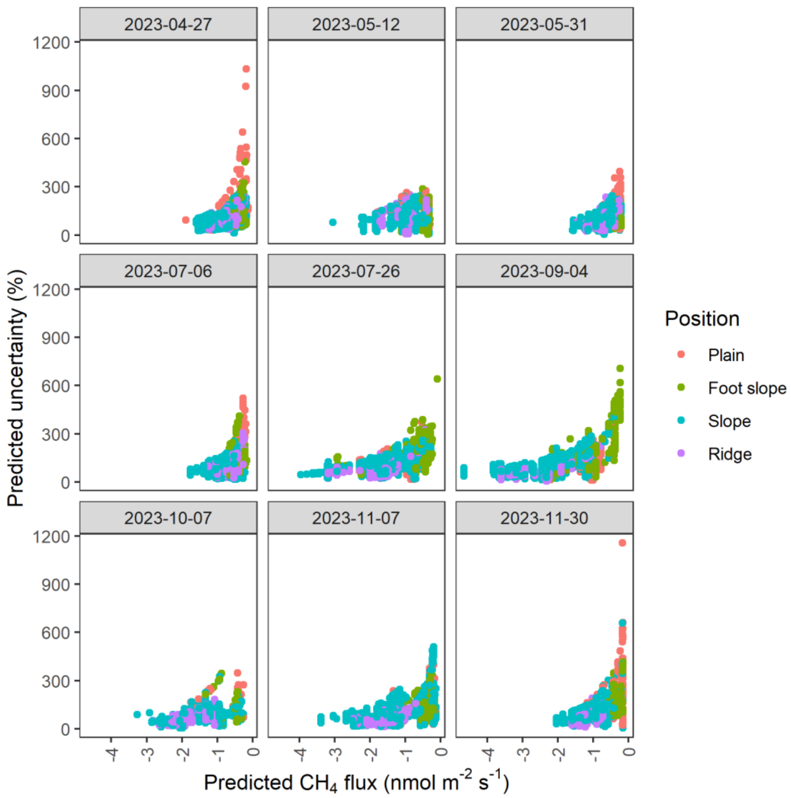

570 **Fig A2. Relationship between predicted uncertainty and predicted CH_4 fluxes. The highest uncertainty is observed for a near-zero prediction.**

https://doi.org/10.5194/egusphere-2025-3449
Preprint. Discussion started: 8 August 2025

Data availability

The data used in this study are available at The Kyoto University Research Information Repository (KURANAI, DOI: to be added)

Author contribution

DE had the original idea of this research. DE and SKP designed the research framework with suggestions from MD. SKP, DE, and KY conducted the vegetation survey and flux measurements. SKP analyzed and performed the modeling under the supervision of DE. SKP wrote the manuscript that was critically reviewed and edited by all co-authors.

Competing interest

The authors declare that they have no conflict of interest.

Acknowledgement

We would like to thank the staff of the Ashiu Forest Station of the Field Science Education and Research Centre, Kyoto University for enabling this research, providing the access to the forest, and for sharing the Digital Elevation Model (DEM) and climate data. We are grateful to Takumi Mochidome for his helpful discussion about GIS and Lucie Bivaud and Makoto Nagasawa for their help during the field survey.

Funding

The research was supported by grants from the Research Institute for Sustainable Humanosphere (RISH), Kyoto University, the Japan Society for the Promotion of Science (KAKENHI Grant no. JP24K01797) and the SPRING fellowship program from Japan Science and Technology (JST SPRING Grant no. JPMJSP2110).

References

Ågren, A. M., Lidberg, W., Strömgren, M., Ogilvie, J., and Arp, P. A.: Evaluating digital terrain indices for soil wetness mapping – a Swedish case study, Hydrol. Earth Syst. Sci., 18, 3623–3634, https://doi.org/10.5194/hess-18-3623-2014, 2014.

Angel, R., Claus, P., and Conrad, R.: Methanogenic archaea are globally ubiquitous in aerated soils and become active under wet anoxic conditions, ISME J., 6, 847–862, https://doi.org/10.1038/ismej.2011.141, 2012.

Aronson, E. L. and Helliker, B. R.: Methane flux in non-wetland soils in response to nitrogen addition: a meta-analysis, Ecology, 91, 3242–3251, https://doi.org/10.1890/09-2185.1, 2010.

Bartoń, K.: MuMIn: Multi-Model Inference, https://doi.org/10.32614/CRAN.package.MuMIn, 2010.

Bates, D., Mächler, M., Bolker, B., and Walker, S.: Fitting linear mixed-effects models using lme4, J. Stat. Soft., 67, https://doi.org/10.18637/jss.v067.i01, 2015.

Bell, J. C., Cunningham, R. L., and Havens, M. W.: Calibration and validation of a soil-landscape model for predicting soil drainage class, Soil Science Soc of Amer J, 56, 1860–1866, https://doi.org/10.2136/sssaj1992.03615995005600060035x, 1992.

Beven, K. J. and Kirkby, M. J.: A physically based, variable contributing area model of basin hydrology / Un modèle à base physique de zone d'appel variable de l'hydrologie du bassin versant, Hydrol. Sci. Bull., 24, 43–69, https://doi.org/10.1080/02626667909491834, 1979.

Bock, M. and Köthe, R.: Predicting the depth of hydromorphic soil characteristics influenced by ground water, SAGA-Seconds Out, 19, 13–22, 2008.

Bodelier, P. L. E. and Laanbroek, H. J.: Nitrogen as a regulatory factor of methane oxidation in soils and sediments, FEMS Microbiol. Ecol., 47, 265–277, https://doi.org/10.1016/S0168-6496(03)00304-0, 2004.

Börjesson, G. and Nohrstedt, H.-Ö.: Fast recovery of atmospheric methane consumption in a Swedish forest soil after single-shot N-fertilization, For. Ecol. Manage., 134, 83–88, https://doi.org/10.1016/S0378-1127(99)00249-2, 2000.

Borken, W., Xu, Y., and Beese, F.: Conversion of hardwood forests to spruce and pine plantations strongly reduced soil methane sink in Germany, Glob Change Biol., 9, 956–966, https://doi.org/10.1046/j.1365-2486.2003.00631.x, 2003.

Breiman, L.: Random Forest, Machine learning, 45, 5–32, https://doi.org/10.1023/A:1010933404324, 2001.

Brumme, R. and Borken, W.: Site variation in methane oxidation as affected by atmospheric deposition and type of temperate forest ecosystem, Glob. Biogeochem. Cycles, 13, 493–501, https://doi.org/10.1029/1998GB900017, 1999.

Burt, R., Reinsch, T. G., and Miller, W. P.: A micro-pipette method for water dispersible clay, Commun. Soil Sci. Plant Anal., 24, 2531–2544, https://doi.org/10.1080/00103629309368975, 1993.

Christiansen, J. R., Levy-Booth, D., Prescott, C. E., and Grayston, S. J.: Microbial and environmental controls of methane fluxes along a soil moisture gradient in a pacific coastal temperate rainforest, Ecosystems, 19, 1255–1270, https://doi.org/10.1007/s10021-016-0003-1, 2016.

Courtois, E. A., Stahl, C., Van Den Berge, J., Bréchet, L., Van Langenhove, L., Richter, A., Urbina, I., Soong, J. L., Peñuelas, J., and Janssens, I. A.: Spatial Variation of Soil CO2, CH4 and N2O Fluxes Across Topographical Positions in Tropical Forests of the Guiana Shield, Ecosystems, 21, 1445–1458, https://doi.org/10.1007/s10021-018-0232-6, 2018.

Du, Z., Riveros-Iregui, D. A., Jones, R. T., McDermott, T. R., Dore, J. E., McGlynn, B. L., Emanuel, R. E., and Li, X.: Landscape position influences microbial composition and function via redistribution of soil water across a watershed, Appl Environ Microbiol, 81, 8457–8468, https://doi.org/10.1128/AEM.02643-15, 2015.

Dutaur, L. and Verchot, L. V.: A global inventory of the soil CH_4 sink, Glob. Biogeochem. Cycles, 21, 2006GB002734, https://doi.org/10.1029/2006GB002734, 2007.

Epron, D., Plain, C., Ndiaye, F.-K., Bonnaud, P., Pasquier, C., and Ranger, J.: Effects of compaction by heavy machine traffic on soil fluxes of methane and carbon dioxide in a temperate broadleaved forest, For. Ecol. Manage., 382, 1–9, https://doi.org/10.1016/j.foreco.2016.09.037, 2016.

Epron, D., Mochidome, T., Tanabe, T., Dannoura, M., and Sakabe, A.: Variability in stem methane emissions and wood methane production of different tree species in a cold temperate mountain forest, Ecosystems, 26, 784–799, https://doi.org/10.1007/s10021-022-00795-0, 2023.

Freeman, T. G.: Calculating catchment area with divergent flow based on a regular grid, Computers & Geosciences, 17, 413–422, https://doi.org/10.1016/0098-3004(91)90048-i, 1991.

Genuer, R., Poggi, J.-M., and Tuleau-Malot, C.: Variable selection using random forests, Pattern Recognit. Lett., 31 (14), 2225–2236, 2010.

Genuer, R., Poggi, J.-M., and Tuleau-Malot, C.: VSURF: An R package for variable selection using random forests, The R Journal, 7, 19, https://doi.org/10.32614/RJ-2015-018, 2015.

Gomez, J., Vidon, P., Gross, J., Beier, C., Caputo, J., and Mitchell, M.: Estimating greenhouse gas emissions at the soil–atmosphere interface in forested watersheds of the US Northeast, Environ. Monit. Assess., 188, 295, https://doi.org/10.1007/s10661-016-5297-0, 2016.

Greenwell, B., M. and Boehmke, B., C.: Variable importance plots—an introduction to the vip package, The R Journal, 12, 343, https://doi.org/10.32614/RJ-2020-013, 2020.

Guckland, A., Flessa, H., and Prenzel, J.: Controls of temporal and spatial variability of methane uptake in soils of a temperate deciduous forest with different abundance of European beech (Fagus sylvatica L.), Soil Biol. Biochem., 41, 1659–1667, https://doi.org/10.1016/j.soilbio.2009.05.006, 2009.

Hirai, H., Araki, S., and Kyuma, K.: Characteristics of brown forest soils developed on the paleozoic shale in northern Kyoto with special reference to their pedogenetic process, Soil Sci. Plant Nutr., 34, 157–170, https://doi.org/10.1080/00380768.1988.10415670, 1988.

Holwerda, F., Scatena, F. N., and Bruijnzeel, L. A.: Throughfall in a Puerto Rican lower montane rain forest: A comparison of sampling strategies, J. Hydrol., 327, 592–602, https://doi.org/10.1016/j.jhydrol.2005.12.014, 2006.

Hu, R., Hirano, T., Sakaguchi, K., Yamashita, S., Cui, R., Sun, L., and Liang, N.: Spatiotemporal variation in soil methane uptake in a cool-temperate immature deciduous forest, Soil Biol. Biochem., 184, 109094, https://doi.org/10.1016/j.soilbio.2023.109094, 2023.

Hütsch, B. W.: Tillage and land use effects on methane oxidation rates and their vertical profiles in soil, Biol. Fertil. Soils., 27, 284–292, https://doi.org/10.1007/s003740050435, 1998.

IPCC: Climate Change 2021 – The Physical Science Basis: Working Group I Contribution to the Sixth Assessment Report of the Intergovernmental Panel on Climate Change, 1st ed., Cambridge University Press, https://doi.org/10.1017/9781009157896, 2023.

Ishihara, M. I., Suzuki, S. N., Nakamura, M., Enoki, T., Fujiwara, A., Hiura, T., Homma, K., Hoshino, D., Hoshizaki, K., Ida, H., Ishida, K., Itoh, A., Kaneko, T., Kubota, K., Kuraji, K., Kuramoto, S., Makita, A., Masaki, T., Namikawa, K., Niiyama, K., Noguchi, M., Nomiya, H., Ohkubo, T., Saito, S., Sakai, T., Sakimoto, M., Sakio, H., Shibano, H., Sugita, H., Suzuki, M., Takashima, A., Tanaka, N., Tashiro, N., Tokuchi, N., Yakushima Forest Environment Conservation Center, Yoshida, T., and Yoshida, Y.: Forest stand structure, composition, and dynamics in 34 sites over Japan, Ecol. Res., 26, 1007–1008, https://doi.org/10.1007/s11284-011-0847-y, 2011.

Ishizuka, S., Sakata, T., and Ishizuka, K.: Methane oxidation in Japanese forest soils, Soil Biol. Biochem., 32, 769–777, https://doi.org/10.1016/S0038-0717(99)00200-X, 2000.

Ishizuka, S., Sakata, T., Sawata, S., Ikeda, S., Sakai, H., Takenaka, C., Tamai, N., Onodera, S., Shimizu, T., Kanna, K., Tanaka, N., and Takahashi, M.: Methane uptake rates in Japanese forest soils depend on the oxidation ability of topsoil, with a new estimate for global methane uptake in temperate forest, Biogeochemistry, 92, 281–295, https://doi.org/10.1007/s10533-009-9293-0, 2009.

Itoh, M., Ohte, N., and Koba, K.: Methane flux characteristics in forest soils under an East Asian monsoon climate, Soil Biol. Biochem., 41, 388–395, https://doi.org/10.1016/j.soilbio.2008.12.003, 2009.

https://doi.org/10.5194/egusphere-2025-3449
Preprint. Discussion started: 8 August 2025

Jacinthe, P. A., Vidon, P., Fisher, K., Liu, X., and Baker, M. E.: Soil methane and carbon dioxide fluxes from cropland and riparian buffers in different hydrogeomorphic settings, J. Environ. Qual., 44, 1080–1090, https://doi.org/10.2134/jeq2015.01.0014, 2015.

Jensen, S., Priemé, A., and Bakken, L.: Methanol improves methane uptake in starved methanotrophic microorganisms, Appl. Environ. Microbiol., 64, 1143–1146, https://doi.org/10.1128/AEM.64.3.1143-1146.1998, 1998.

Jeong, G., Oeverdieck, H., Park, S. J., Huwe, B., and Ließ, M.: Spatial soil nutrients prediction using three supervised learning methods for assessment of land potentials in complex terrain, Catena, 154, 73–84, https://doi.org/10.1016/j.catena.2017.02.006, 2017.

Jevon, F. V., Gewirtzman, J., Lang, A. K., Ayres, M. P., and Matthes, J. H.: Tree species effects on soil CO_2 and CH_4 fluxes in a mixed temperate forest, Ecosystems, https://doi.org/10.1007/s10021-023-00852-2, 2023.

Kagotani, Y., Hamabata, E., and Nakajima, T.: Seasonal and spatial variations and the effects of clear-cutting in the methane absorption rates of a temperate forest soil, Nutr. Cycl. Agroecosystems, 59, 169–175, https://doi.org/10.1023/A:1017554031367, 2001.

Kaiser, K. E., McGlynn, B. L., and Dore, J. E.: Landscape analysis of soil methane flux across complex terrain, Biogeosciences, 15, 3143–3167, https://doi.org/10.5194/bg-15-3143-2018, 2018.

Kemppinen, J., Niittynen, P., Riihimäki, H., and Luoto, M.: Modelling soil moisture in a high-latitude landscape using LiDAR and soil data, Earth Surf. Processes Landf., 43, 1019–1031, https://doi.org/10.1002/esp.4301, 2018.

King, G. M. and Schnell, S.: Ammonium and nitrite inhibition of methane oxidation by *Methylobacter albus* BG8 and *Methylosinus trichosporium* OB3b at low methane concentrations, Appl Environ. Microbiol., 60, 3508–3513, https://doi.org/10.1128/aem.60.10.3508-3513.1994, 1994.

Kohler, M. A. and Linsley, R. K.: Predicting the Runoff from Storm Rainfall, US department of commerce, Weather Bureau, 20, 1951.

Kravchenko, A. N., Bollero, G. A., Omonode, R. A., and Bullock, D. G.: Quantitative mapping of soil drainage classes using topographical data and soil electrical conductivity, Soil Sci. Soc. Am. J., 66, 235–243, https://doi.org/10.2136/sssaj2002.2350, 2002.

Kruse, C. W., Moldrup, P., and Iversen, N.: Modeling diffusion and reaction in soils: II. atmospheric methane diffusion and consumption in a forest soil, Soil Sci., 161, 355–365, https://doi.org/10.1097/00010694-199606000-00002, 1996.

Kuhn, M. and Johnson, K.: Applied Predictive Modeling, Springer New York, New York, NY, https://doi.org/10.1007/978-1-4614-6849-3, 2013.

Kuznetsova, A., Brockhoff, P. B., and Christensen, R. H. B.: lmerTest package: tests in linear mixed effects models, J. Stat. Soft., 82, https://doi.org/10.18637/jss.v082.i13, 2017.

Lee, J., Oh, Y., Lee, S. T., Seo, Y. O., Yun, J., Yang, Y., Kim, J., Zhuang, Q., and Kang, H.: Soil organic carbon is a key determinant of CH_4 sink in global forest soils, Nat. Commun., 14, 3110, https://doi.org/10.1038/s41467-023-38905-8, 2023.

Lenth, R. V.: emmeans: Estimated Marginal Means, aka Least-Squares Means, https://doi.org/10.32614/cran.package.emmeans, 2017.

Lundbäck, M., Persson, H., Häggström, C., and Nordfjell, T.: Global analysis of the slope of forest land, Forestry, 94, 54–69, https://doi.org/10.1093/forestry/cpaa021, 2021.

Luo, G. J., Kiese, R., Wolf, B., and Butterbach-Bahl, K.: Effects of soil temperature and moisture on methane uptake and nitrous oxide emissions across three different ecosystem types, Biogeosciences, 10, 3205–3219, https://doi.org/10.5194/bg-10-3205-2013, 2013.

Martinson, G. O., Müller, A. K., Matson, A. L., Corre, M. D., and Veldkamp, E.: Nitrogen and phosphorus control soil methane uptake in tropical montane forests, JGR Biogeosciences, 126, e2020JG005970, https://doi.org/10.1029/2020JG005970, 2021.

Meinshausen, N.: Quantile Regression Forests, J. Mach. Learn. Res., 7, 983–999, 2006.

Meinshausen, N.: quantregForest: Quantile Regression Forests, https://doi.org/10.32614/CRAN.package.quantregForest, 2017.

Miller, B. A., Koszinski, S., Wehrhan, M., and Sommer, M.: Impact of multi-scale predictor selection for modeling soil properties, Geoderma, 239–240, 97–106, https://doi.org/10.1016/j.geoderma.2014.09.018, 2015.

Mochizuki, Y., Koba, K., and Yoh, M.: Strong inhibitory effect of nitrate on atmospheric methane oxidation in forest soils, Soil Biol. Biochem., 50, 164–166, https://doi.org/10.1016/j.soilbio.2012.03.013, 2012.

Murphy, P. N. C., Ogilvie, J., Meng, F.-R., White, B., Bhatti, J. S., and Arp, P. A.: Modelling and mapping topographic variations in forest soils at high resolution: A case study, Ecol. Model., 222, 2314–2332, https://doi.org/10.1016/j.ecolmodel.2011.01.003, 2011.

Nakamura, Y. and Krestov, P. V.: Coniferous forests of the temperate zone of asia, Ecosystems of the world ser. conifferous forests, 6, 163–220, 2005.

Osborne, B. B., Nasto, M. K., Asner, G. P., Balzotti, C. S., Cleveland, C. C., Sullivan, B. W., Taylor, P. G., Townsend, A. R., and Porder, S.: Climate, topography, and canopy chemistry exert hierarchical control over soil N cycling in a neotropical lowland forest, Ecosystems, 20, 1089–1103, https://doi.org/10.1007/s10021-016-0095-7, 2017.

Pachepsky, Ya. A., Timlin, D. J., and Rawls, W. J.: Soil Water Retention as Related to Topographic Variables, Soil Science Soc of Amer J, 65, 1787–1795, https://doi.org/10.2136/sssaj2001.1787, 2001.

Pinheiro, J., R Core Team, and Bates, D.: nlme: Linear and Nonlinear Mixed Effects Models, https://doi.org/10.32614/cran.package.nlme, 1999.

Praeg, N., Wagner, A. O., and Illmer, P.: Plant species, temperature, and bedrock affect net methane flux out of grassland and forest soils, Plant Soil., 410, 193–206, https://doi.org/10.1007/s11104-016-2993-z, 2017.

Quebbeman, A. W., Menge, D. N. L., Zimmerman, J., and Uriarte, M.: Topography and tree species improve estimates of spatial variation in soil greenhouse gas fluxes in a subtropical forest, Ecosystems, 25, 648–660, https://doi.org/10.1007/s10021-021-00677-x, 2022.

R Core Team: A language and environment for statistical computing, R: A language and environment for statistical computing, 2024.

Räsänen, A., Manninen, T., Korkiakoski, M., Lohila, A., and Virtanen, T.: Predicting catchment-scale methane fluxes with multi-source remote sensing, Landscape Ecol., 36, 1177–1195, https://doi.org/10.1007/s10980-021-01194-x, 2021.

Roberts, D. R., Bahn, V., Ciuti, S., Boyce, M. S., Elith, J., Guillera-Arroita, G., Hauenstein, S., Lahoz-Monfort, J. J., Schröder, B., Thuiller, W., Warton, D. I., Wintle, B. A., Hartig, F., and Dormann, C. F.: Cross-validation strategies for data with temporal, spatial, hierarchical, or phylogenetic structure, Ecography, 40, 913–929, https://doi.org/10.1111/ecog.02881, 2017.

https://doi.org/10.5194/egusphere-2025-3449
Preprint. Discussion started: 8 August 2025

Saunois, M., Stavert, A. R., Poulter, B., Bousquet, P., Canadell, J. G., Jackson, R. B., Raymond, P. A., Dlugokencky, E. J., Houweling, S., Patra, P. K., Ciais, P., Arora, V. K., Bastviken, D., Bergamaschi, P., Blake, D. R., Brailsford, G., Bruhwiler, L., Carlson, K. M., Carrol, M., Castaldi, S., Chandra, N., Crevoisier, C., Crill, P. M., Covey, K., Curry, C. L., Etiope, G., Frankenberg, C., Gedney, N., Hegglin, M. I., Höglund-Isaksson, L., Hugelius, G., Ishizawa, M., Ito, A., Janssens-Maenhout, G., Jensen, K. M., Joos, F., Kleinen, T., Krummel, P. B., Langenfelds, R. L., Laruelle, G. G., Liu, L., Machida, T., Maksyutov, S., McDonald, K. C., McNorton, J., Miller, P. A., Melton, J. R., Morino, I., Müller, J., Murguia-Flores, F., Naik, V., Niwa, Y., Noce, S., O'Doherty, S., Parker, R. J., Peng, C., Peng, S., Peters, G. P., Prigent, C., Prinn, R., Ramonet, M., Regnier, P., Riley, W. J., Rosentreter, J. A., Segers, A., Simpson, I. J., Shi, H., Smith, S. J., Steele, L. P., Thornton, B. F., Tian, H., Tohjima, Y., Tubiello, F. N., Tsuruta, A., Viovy, N., Voulgarakis, A., Weber, T. S., Van Weele, M., Van Der Werf, G. R., Weiss, R. F., Worthy, D., Wunch, D., Yin, Y., Yoshida, Y., Zhang, W., Zhang, Z., Zhao, Y., Zheng, B., Zhu, Q., Zhu, Q., and Zhuang, Q.: The Global Methane Budget 2000–2017, Earth Syst. Sci. Data, 12, 1561–1623, https://doi.org/10.5194/essd-12-1561-2020, 2020.

Schoener, G. and Stone, M. C.: Monitoring soil moisture at the catchment scale – A novel approach combining antecedent precipitation index and radar-derived rainfall data, J. Hydrol., 589, 125155, https://doi.org/10.1016/j.jhydrol.2020.125155, 2020.

Semrau, J. D., DiSpirito, A. A., and Vuilleumier, S.: Facultative methanotrophy: false leads, true results, and suggestions for future research: Facultative methanotrophy, FEMS Microbiol. Lett., 323, 1–12, https://doi.org/10.1111/j.1574-6968.2011.02315.x, 2011.

Sidle, R. C., Tsuboyama, Y., Noguchi, S., Hosoda, I., Fujieda, M., and Shimizu, T.: Stormflow generation in steep forested headwaters: a linked hydrogeomorphic paradigm, Hydrol. Process., 14, 369–385, https://doi.org/10.1002/(SICI)1099-1085(20000228)14:3<369::AID-HYP943>3.0.CO;2-P, 2000.

Tateno, R. and Takeda, H.: Forest structure and tree species distribution in relation to topography-mediated heterogeneity of soil nitrogen and light at the forest floor, Ecol. Res., 18, 559–571, https://doi.org/10.1046/j.1440-1703.2003.00578.x, 2003.

Ueda, S., Ando, M., and Kanzaki, K.: Forest soil surveys of the Kyoto University Forest in Ashiu. II. Soil types, grain size, and chemical and physical properties of soils, Bulletin of the Kyoto University Forests, 65, 94–112, 1993.

Vainio, E., Peltola, O., Kasurinen, V., Kieloaho, A.-J., Tuittila, E.-S., and Pihlatie, M.: Topography-based statistical modelling reveals high spatial variability and seasonal emission patches in forest floor methane flux, Biogeosciences, 18, 2003–2025, https://doi.org/10.5194/bg-18-2003-2021, 2021.

Veldkamp, E., Koehler, B., and Corre, M. D.: Indications of nitrogen-limited methane uptake in tropical forest soils, Biogeosciences, 10, 5367–5379, https://doi.org/10.5194/bg-10-5367-2013, 2013.

Virkkala, A.-M., Niittynen, P., Kemppinen, J., Marushchak, M. E., Voigt, C., Hensgens, G., Kerttula, J., Happonen, K., Tyystjärvi, V., Biasi, C., Hultman, J., Rinne, J., and Luoto, M.: High-resolution spatial patterns and drivers of terrestrial ecosystem carbon dioxide, methane, and nitrous oxide fluxes in the tundra, Biogeosciences, 21, 335–355, https://doi.org/10.5194/bg-21-335-2024, 2024.

Wang, J. M., Murphy, J. G., Geddes, J. A., Winsborough, C. L., Basiliko, N., and Thomas, S. C.: Methane fluxes measured by eddy covariance and static chamber techniques at a temperate forest in central Ontario, Canada, Biogeosciences, 10, 4371–4382, https://doi.org/10.5194/bg-10-4371-2013, 2013.

https://doi.org/10.5194/egusphere-2025-3449
Preprint. Discussion started: 8 August 2025

Wang, L. and Liu, H.: An efficient method for identifying and filling surface depressions in digital elevation models for hydrologic analysis and modelling, Int. J. Geogr. Inf. Sci., 20, 193–213, https://doi.org/10.1080/13658810500433453, 2006.

Warner, D. L., Vargas, R., Seyfferth, A., and Inamdar, S.: Transitional slopes act as hotspots of both soil CO_2 emission and CH_4 uptake in a temperate forest landscape, Biogeochemistry, 138, 121–135, https://doi.org/10.1007/s10533-018-0435-0, 2018.

Warner, D. L., Guevara, M., Inamdar, S., and Vargas, R.: Upscaling soil-atmosphere CO_2 and CH_4 fluxes across a topographically complex forested landscape, Agric. For. Meteorol., 264, 80–91, https://doi.org/10.1016/j.agrformet.2018.09.020, 2019.

West, A. E. and Schmidt, S. K.: Acetate stimulates atmospheric CH_4 oxidation by an alpine tundra soil, Soil Biol. Biochem., 31, 1649–1655, https://doi.org/10.1016/S0038-0717(99)00076-0, 1999.

Yamao, M., Sidle, R. C., Gomi, T., and Imaizumi, F.: Characteristics of landslides in unwelded pyroclastic flow deposits, southern Kyushu, Japan, Nat. Hazards Earth Syst. Sci., 16, 617–627, https://doi.org/10.5194/nhess-16-617-2016, 2016.

Yu, L., Huang, Y., Zhang, W., Li, T., and Sun, W.: Methane uptake in global forest and grassland soils from 1981 to 2010, Sci. Total Environ., 607–608, 1163–1172, https://doi.org/10.1016/j.scitotenv.2017.07.082, 2017.

Yu, L., Zhu, J., Ji, H., Bai, X., Lin, Y., Zhang, Y., Sha, L., Liu, Y., Song, Q., Dörsch, P., Mulder, J., and Zhou, W.: Topography-related controls on N_2O emission and CH_4 uptake in a tropical rainforest catchment, Sci. Total Environ., 775, 145616, https://doi.org/10.1016/j.scitotenv.2021.145616, 2021.

Zevenbergen, L. W. and Thorne, C. R.: Quantitative analysis of land surface topography, Earth Surf. Processes Landf., 12, 47–56, https://doi.org/10.1002/esp.3290120107, 1987.